

Article

Rare Earth Oxide CeO₂ Decorated Graphene Nanoplatelets-Reinforced 2024 Aluminum Alloy Matrix Composites Fabricated by Pressure Sintering Process

Zhenghua Guo, Surui Li, Qingjie Wu * and Ning Li

Department of Materials Processing Engineering, School of Aeronautic Manufacturing Engineering, Nanchang Hangkong University, Nanchang 330063, China; guozh1972@163.com (Z.G.); lisuirui0123@163.com (S.L.); lining@nchu.edu.cn (N.L.)

* Correspondence: 70801@nchu.edu.cn; Tel.: +86-0791-8386-3028

Abstract: In this study, graphene nanoplatelets (GNPs) decorated rare earth oxide CeO₂ (CeO₂@GNPs) were synthesized by alcohol thermal reaction method and used to reinforce GNPs/2024Al composites fabricated by a pressure sintering process. The results indicated that the decorating CeO₂ particles could further promote the dispersion of the GNPs as well the binding of GNPs to the matrix. As a result, the as-prepared 0.5 wt.% CeO₂@GNPs/2024Al composites exhibited yield strength and tensile strength increased by 21.1% and 24.7% compared to these of the matrix, respectively. It is better than the mechanical strength values of the composite enforced with the raw GNPs of the same quality. The optimization of GNPs dispersibility and interfacial bonding with Al matrix promotes its effective role in load-bearing strengthening.

Keywords: aluminum matrix composites (AMCs); graphene nano-platelets; rare earth oxide; mechanical properties



Citation: Guo, Z.; Li, S.; Wu, Q.; Li, N. Rare Earth Oxide CeO₂ Decorated Graphene Nanoplatelets-Reinforced 2024 Aluminum Alloy Matrix Composites Fabricated by Pressure Sintering Process. *Appl. Sci.* **2021**, *11*, 11177. <https://doi.org/10.3390/app112311177>

Academic Editor: Chiara Soffritti

Received: 22 October 2021

Accepted: 23 November 2021

Published: 25 November 2021

Publisher's Note: MDPI stays neutral with regard to jurisdictional claims in published maps and institutional affiliations.



Copyright: © 2021 by the authors. Licensee MDPI, Basel, Switzerland. This article is an open access article distributed under the terms and conditions of the Creative Commons Attribution (CC BY) license (<https://creativecommons.org/licenses/by/4.0/>).

1. Introduction

Since graphene was successfully separated in 2004, it has attracted attention due to its excellent tensile properties, strength, stiffness, and attractive functional properties such as high thermal conductivity and electrical conductivity [1–7]. Graphene or GNPs is considered to be an effective reinforcing agent for composite materials. The unique two-dimensional structure makes it have a larger specific surface area and provides more interfaces and sufficient load transfer substrates. Therefore, GNPs have been used as an important new nano-scale reinforcement material in the field of structural and functional composites [8–10].

Particularly, GNPs have often been used as an effective reinforcement to develop polymer-based composites. In the field of GNPs reinforced metal matrix composites, the research on Al-based alloys as the matrix material is more common [11–13]. Jianchao Li, et al. [14] studied the effect of heat treatment on the strengthening mechanism of GNP/Al composites. Abhishek SHARMA et al. [15] successfully prepared the GNPs/Al6061/SiC composite via friction stir processing. Nanoindentation results revealed a remarkable 207% increment in surface nano-hardness of Al–SiC–GNPs composite compared to Al6061 alloy matrix. Jun-jie Xiong [16] prepared GNPs reinforced ADC12 aluminum matrix composites using high-energy ultrasonic casting technology. Respectively, the tensile strength, yield strength, and microhardness of the composite produced were increased by 30.5%, 42.7%, and 34.8%, compared with those of the matrix due to the addition of GNPs. In addition, the OM images showed that the addition of GNPs has the effect of promoting the refinement of the matrix grains. The results of such literature all revealed the fact that GNPs could be an effective reinforcement to improve the mechanical properties of the aluminum matrix.

However, despite the developments in the field of nano-carbon reinforced aluminum-based materials, there are still some major challenges in the manufacture of graphene-

reinforced metal matrix composites (GRMMC). The force between van der Waals graphene sheets promotes its tendency to agglomerate and the poor bonding wettability with the matrix weakens the load transfer effect during the deformation of the composites [17].

In order to solve those challenges above, the surface modification techniques combined with pressure sintering were used in the field of nano-carbon reinforcement by materials scientists. SiC@CNTs were prepared by Yongha Park et al. [18] and used as the reinforcement of the matrix alloys. The report showed that the presence of the SiC decorating layer resulted in an improvement of the wettability. Similarly, it was reported [19] that interfacial bonding could be effectively improved by decorating nickel oxide (NiO) on the CNTs. The microstructure exhibited that the reinforcement NiO@CNTs shows a better efficiency of grain refinement for the as-casted Mg alloys and dispersion compared with the addition of CNTs. It means that the mechanical properties of composites were further improved. These reports suggest that the surface modification technology may be beneficial to the improvement of the interfacial bonding and the dispensability of the nano-carbon materials. However, there are still few investigations on aluminum composites reinforced with graphene-modified by surface decoration technology.

In the present work, 2024 aluminum matrix alloy reinforced with GNPs (CeO_2 @GNPs) decorated with rare earth oxide particles CeO_2 and purified GNPs were prepared by hot pressing sintering. The comparative experiments were designed to explore the effect of rare earth oxide decorated GNPs on the mechanical properties and the microstructure of the matrix. Meanwhile, the fracture behavior and strengthening mechanism of CeO_2 @GNPs/2024 AL composites were systematically investigated in detail.

2. Materials and Methods

2.1. Material

GNPs with a purity of 99.0% provided by Chengdu Zhongke Group was used as the starting materials to produce the reinforcement CeO_2 @GNPs. Figure 1 shows the SEM image of the typical lamellar morphology of GNPs obtained from a field emission scanning electron microscope (Quanta200F EDAX). The base material in this study was 2024 aluminum alloy powders provided by Hunan Tianjiu, (purity is 99.7%, 600~800 mesh in diameter), the chemical composition of 2024 alloy is shown in Table 1.

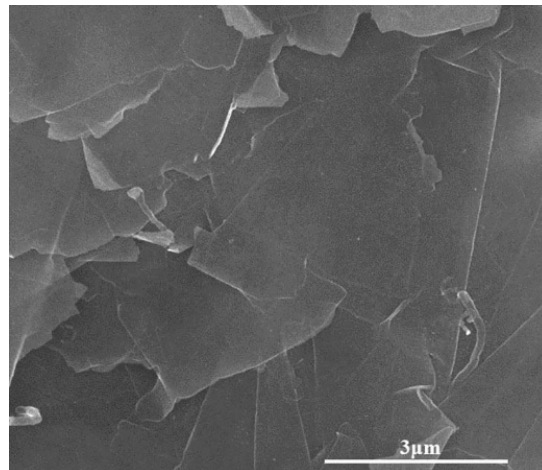


Figure 1. SEM image of the multilayer microstructure morphology of graphene.

Table 1. Chemical composition of 2024 aluminum alloy.

Type	Cu	Mg	Fe	Zn	Al
Wt pct	3.8~5.0	1.2~1.8	0.5	0.25	Bal.

2.2. Procedure

The decorating process: the acidified graphene (0.1 g) was placed into pure analytical alcohol (50 mL) and subjected to ultrasonic treatment to form a suspension. Then, a small amount of $\text{Ce}(\text{NO}_3)_3$ was put into this suspension and continued to sonicate for 12 h, where the molar ratio of $\text{Ce}(\text{NO}_3)_3$ to graphene was 0.08:1. After that, slowly drip an appropriate amount of ammonia into the mixture until the PH of the solution is 8. The mixed solution was transferred to an autoclave and heated in a muffle furnace for 8 h and then cooled to room temperature with the furnace. The reaction temperature was set to 190 °C. Subsequently, the powder precursor in the solution was obtained by a centrifugal process and dried at 90 °C for 24 h. The resulting powder precursor was heated in a roasting furnace for 1 h to obtain GNPs decorated rare earth oxide CeO_2 material (CeO_2 -GNPs).

Preparation of composites: Different types of GNPs together with the as-received Al powders were mixed through via high energy ball milling (HEBM) process under Ar atmosphere, as schematically shown in Figure 2. 0.5 wt.% GNPs, 99.2 wt.% Al powders and 0.3 wt.% stearic acids were placed in stainless steel jars containing quartz milling balls of 5 mm diameter. The ratio of balls to powder ratio was 10:1. The milling process was completed using a planetary ball mill at 400 rpm for varying milling times up to 2 h. Then, the starting powders were sintered by a hot press sintering system at a temperature of 595 °C for 2 h in a vacuum of 10^{-3} torr under a pressure of 23 MPa. The heating rate was maintained at 100 °C/min. In this study, the matrix 2024Al alloy was also prepared by the same procedure for comparison.

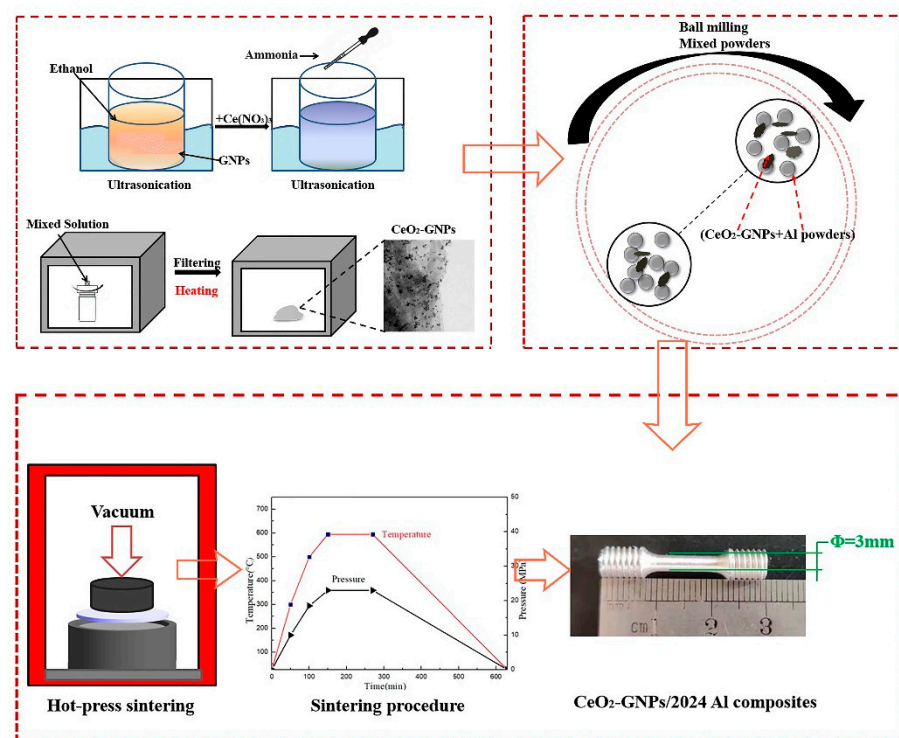


Figure 2. Schematic diagram of the preparation process for GNPs@ CeO_2 /2024Al composites.

Subsequently, optical microscope (Nikon eclipse, MA-200), environmental scanning electron microscope (Quanta200F EDAX), and transmission electron microscope (TEM, Jeol JEM-2100) were used to observe the microstructure of the prepared composite samples. In addition, the prepared samples of the composites fabricated were measured for their hardness and tensile properties by using a micro-Vickers hardness tester (HVS-1000A) and a universal tensile testing machine (Sansi JXYA-105). Vickers hardness test was performed on the polished sample, the loading force was 0.3 kg, and the pressure was held for 15 s. For the tensile tests, the tensile rate was set to 0.5 mm/min. In order to reduce errors,

10 indentation inspection tests were required for each hardness pattern. The tensile test of each material was carried out for 6 repetitions to ensure the correct change trend of the properties obtained.

3. Results

3.1. Material Characterization

Figure 3a shows the TEM image of the CeO₂ surface-decorated GNPs. It can be seen from the image that the surface of GNPs changed considerably after the surface decorating process. From the enlarged image shown in Figure 3b, it can be seen that even after the ultrasonic pretreatment for the TEM test, these generated particles are still tightly adhered to and distributed on the surface of the GNPs. This implies the existence of strong interface bonding [20]. The corresponding EDX spectrum, as shown in Figure 3d, indicates that the particles mainly consisted of Ce and O. Close examination of the rare earth oxides on the surface of the GNPs (Figure 3b) shows a d-spacing with an observed fringe separation of 0.31~0.32 nm. Consistent with the interlayer separations of the (111) [21] crystal plane of CeO₂ (Figure 3c). Therefore, it could be confirmed that CeO₂ particles have been successfully generated and decorated on the surface of GNPs.

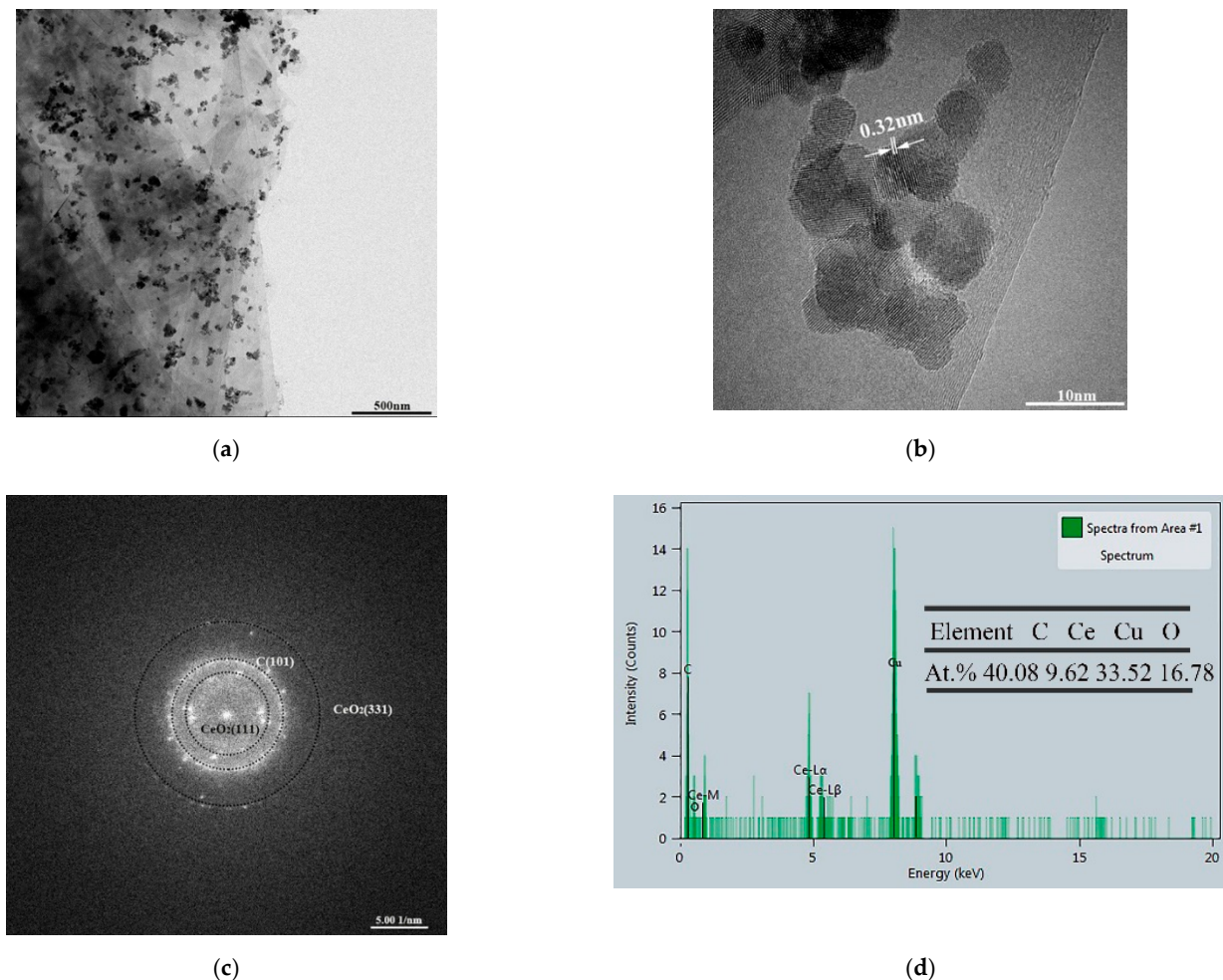


Figure 3. TEM photographs of CeO₂-GNPs: (a) TEM and (b) HRTEM images of CeO₂-GNPs; (c) SAED patterns; (d) corresponding EDX result of the nanoparticles.

To assess the damage degree of the surface-decorated and ball milling process to the GNPs. The comparison of the Raman spectra of original GNPs and Al-CeO₂-GNPs mixture after ball milling is shown in Figure 4. The better the structural integrity of GNPs, the

smaller the ID/IG value in general. In this study, it is mainly to show the change of its value after processing. The results show that the apparent peaks are located at $\sim 1350\text{ cm}^{-1}$ and $\sim 1580\text{ cm}^{-1}$ [22], corresponding to the D-band and G band of GNPs, respectively. The calculated values (ID/IG) were 0.66 and 0.82, which means that even after the ball milling process, these characteristic values only slightly increased. Namely, compared with the original GNPs, the ball milling process only caused slight damage to the surface of GNPs. The structural integrity of the GNPs in the mixed powder was not damaged.

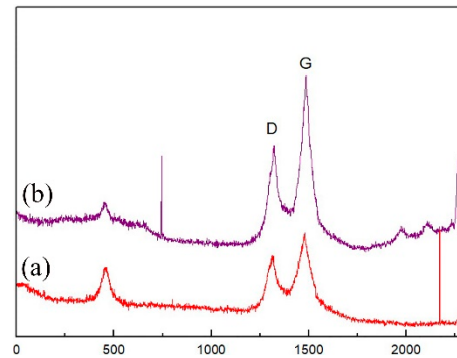


Figure 4. Raman spectra of origin GNPs (a) and Al-GNPs (b).

The optical micrograph and grain size distribution of 2024 matrix alloy, 0.5 wt.% GNPs/2024Al and CeO₂-GNPs/2024Al composites are shown in Figure 5. The average values of the grains are also labeled in Figure 5d–f. The comparison of Figure 5a–c reveals that the grains of matrix alloy was refined after adding an appropriate amount of GNPs. This phenomenon is usually caused by the GNPs distributed in the grain boundaries hindering the growth of the grains [23]. On the other hand, it can be observed through Figure 5b,c that the grain size of the composite prepared by adding the reinforcement CeO₂-GNPs was smaller than that of adding raw GNPs. As can be seen from Figure 5e,f, the average grain size of the 0.5 wt.% GNPs/2024Al composite was 26.4 μm , while that size of the 0.5 wt.% CeO₂-GNPs/2024Al composite was further reduced to 22.9 μm . In addition, there were fewer micropores revealed on the surface of the 0.5 wt.% CeO₂-GNPs/2024Al composite compared with the others. Generally, the micropores structure is considered to be the agglomerations of GNPs at the grain boundaries. An appropriate amount of GNPs has a grain refinement effect on the matrix alloy existing in the grain boundary, as mentioned above. However, a large amount of agglomerated GNPs impedes the continuity of the metal material, resulting in the deterioration of the mechanical properties of the composites [24]. These observations could be attributed to the decorating process that optimizes the wettability of GNPs with 2024 alloy and, therefore, improves the dispersibility of the GNPs in the matrix. The improvement of the wettability between the GNPs and the matrix promotes the combination of GNPs and alloy, which leads to a reduction in structural defects during the process.

Figure 6 shows the TEM and HRTEM analysis of CeO₂-GNPs/2024Al composites prepared with this current process. It can be seen from Figure 6a,b that the shape of some phases is similar to the multi-layer structure of GNPs. In addition, the obvious boundary lines of the GNPs in the matrix were clearly visible without obvious pores and defects such as cracks, as shown in Figure 6b. This indicates that a sound interface between the GNP and the Al matrix, which is beneficial to promote the improvement of the mechanical properties of composites. Moreover, it is worth noting that some granular sphere nanoparticles can also be found on the surface of GNPs as shown in the HRTEM image (Figure 6c). The d-spacing of these nanoparticles provided by SAED pattern (Figure 6d) was 1.56 nm and 0.31 nm, corresponding to the (222) and (111) planes of CeO₂. This means that the decorating CeO₂ particles can still remain on the surface of the GNPs even after the composite was prepared by the pressure sintering process.

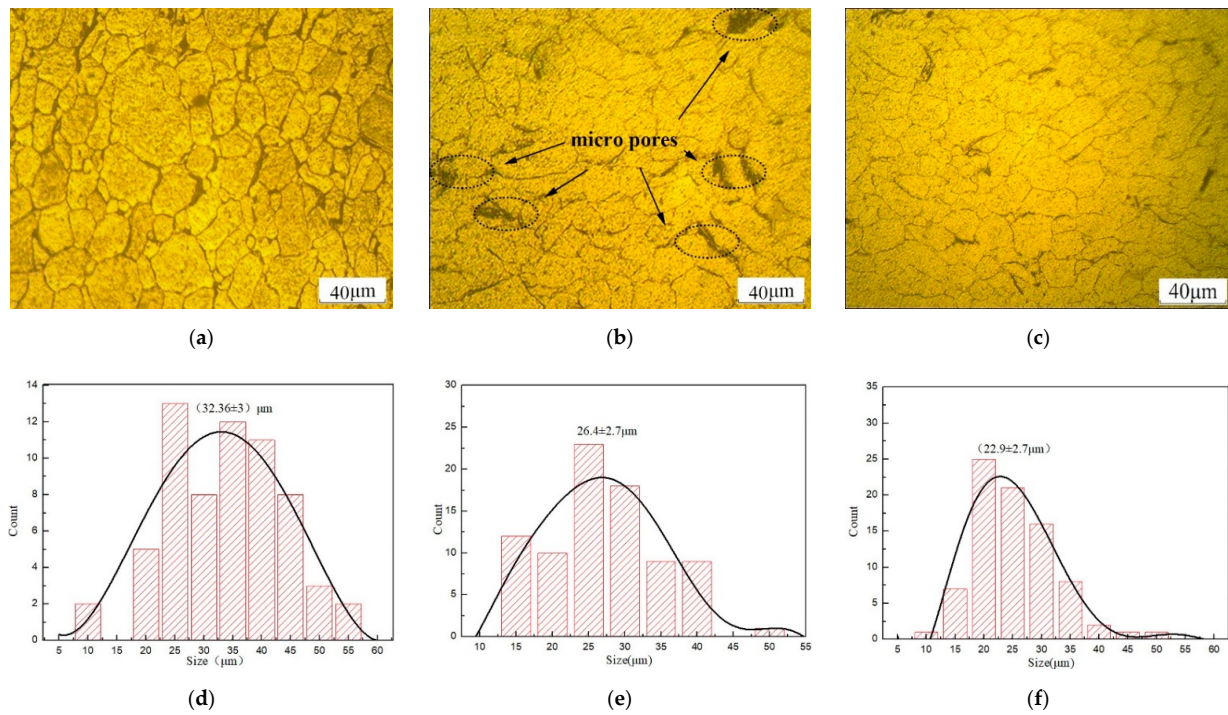


Figure 5. Microstructures and the grain sizes distribution of the matrix and 2024Al with different reinforcement: (a,d) the matrix; (b,e) GNPs/2024Al composites; (c,f) CeO₂-GNPs/2024Al composites.

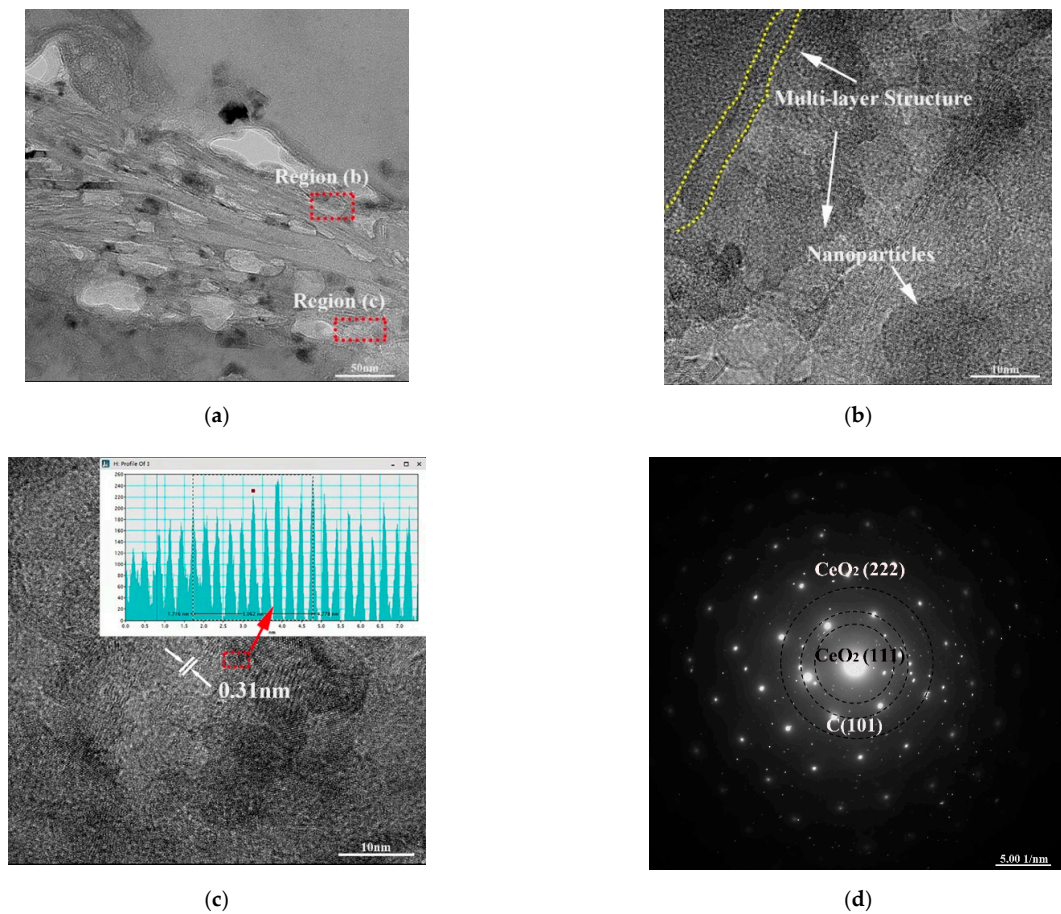


Figure 6. TEM images of CeO₂-GNPs/2024Al composite: (a) high-angle annular dark-field image; (b,c) HRTEM image of regions; (c) SAED pattern of Region A; (d) SAED patterns of region (c).

Figure 7 shows the EDX-mapping images of different elements in 0.5 wt.% GNPs/2024Al composite fabricated. It can be clearly seen from the images that the distribution of Al, Mg, Cu, and Ce elements, as well as the GNPs exhibiting a wrinkled morphology. It is consistent with the TEM images exhibited in Figure 6. It can also be noticed that Mg and Cu elements are relatively easy to accumulate near GNPs. In addition, Ce elements were detected near the GNPs distribution area, as shown in Figure 7. This proves the conclusion obtained as mentioned before: the rare earth oxide modification CeO_2 particles on the surfaces of the GNPs in the composite fabricated are retained to a certain extent.

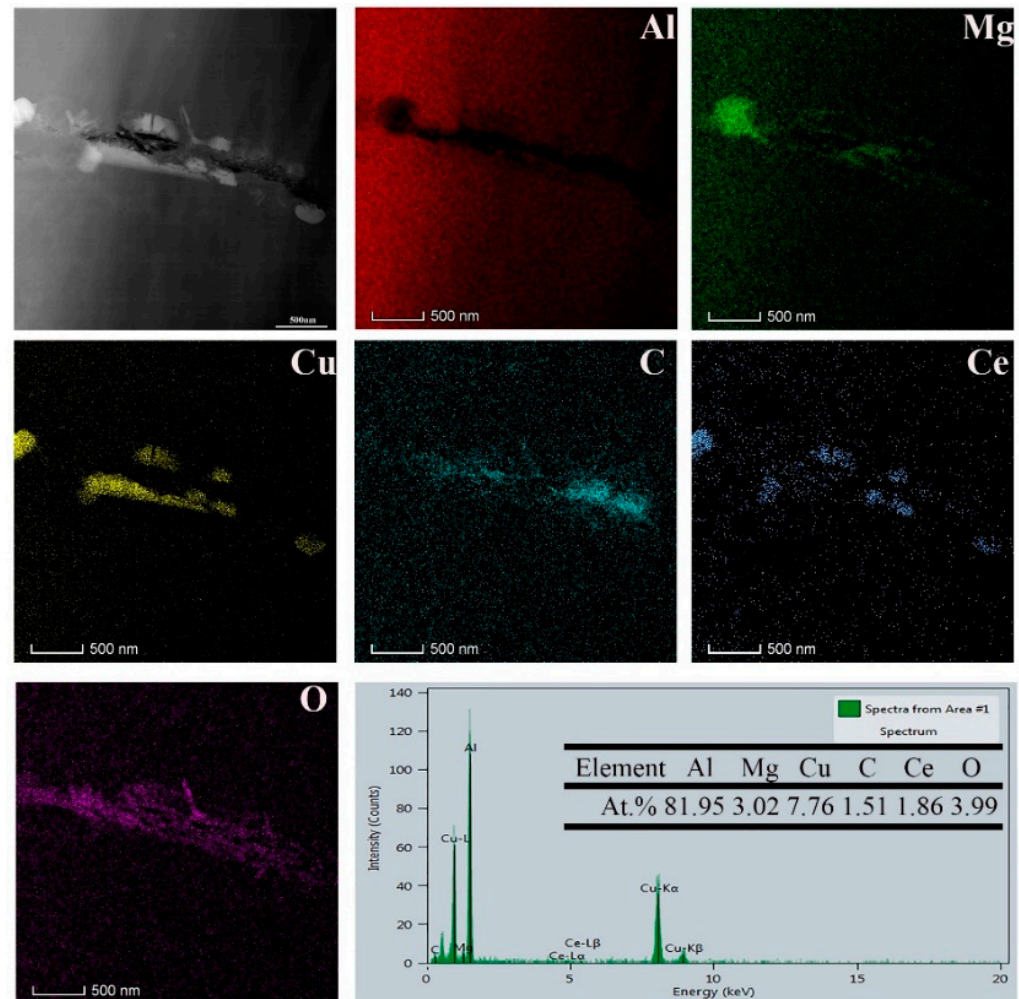


Figure 7. Mapping analysis of the 0.5 wt.% GNPs/2024Al composite fabricated.

3.2. Material Properties

The representative tensile stress-strain curve of the prepared composites and 2024Al matrix is shown in Figure 8. Correspondingly, the yield strength (YS), ultimate tensile strength (UTS), and microhardness obtained from the test are provided in Table 2. It can be seen that the mechanical properties of the composites were significantly improved after adding an appropriate amount of GNPs. The average UTS and YS exhibited were approximately 170.6 MPa and 257.4 MPa, which represent an increase of 12.2% and 18% compared to the matrix value, respectively. In addition, the composite fabricated shows better mechanical properties than the original 0.5 wt.% GNPs/2024Al composite when the reinforcement is replaced with modified GNPs. The YS and UTS of the nanocomposite reinforced with CeO_2 -GNPs were 184.1 MPa and 271.8 MPa, increasing by 21.1% and 24.7%, as compared to the matrix. The carbon-based reinforcement with coated particles

provides a pinning effect on the dislocation during the deformation process, leading to further improvement in the mechanical properties of the composites [25].

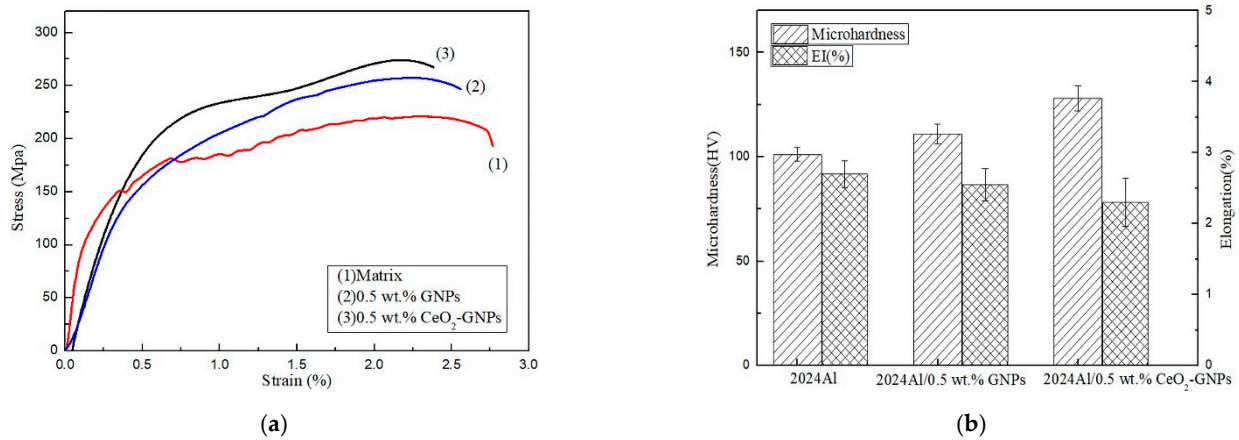


Figure 8. Tensile strain-stress curves (a) and microhardness (b) of the composites fabricated and 2024 Al alloy matrix.

Table 2. Corresponding mechanical properties of composites prepared.

Composites	YS (MPa)	UTS (MPa)	Microhardness (Hv)
2024Al	152	218	101.2
2024Al composite/0.5 wt.% GNPs	170.6	257.4	111
2024Al composite/0.5 wt.% CeO ₂ -GNPs	184.1	271.8	128

Figure 9a–d shows the typical fracture morphology and EDX results of composites reinforced with GNPs and CeO₂-GNPs. The fracture morphology of the 0.5 wt.% GNPs/2024Al composite is mainly composed of cleavage fracture, torn edges, and lots of platforms, as shown in Figure 9a. It means that the fracture of the composite is a mainly brittle fracture. When the reinforcement has been replaced by CeO₂-GNPs, the number of brittle platforms areas shows a decreasing trend, as can be seen in Figure 9d. Furthermore, it can be clearly observed from the microstructure comparison in Figure 9b,d that there are more obvious gaps between the original GNP_s and the matrix. Moreover, the decorated GNPs have a better bonding with the matrix compared with the original GNPs. It means the interface bonding between GNPs and the matrix has been improved due to the surface decoration effect of the rare earth oxide CeO₂.

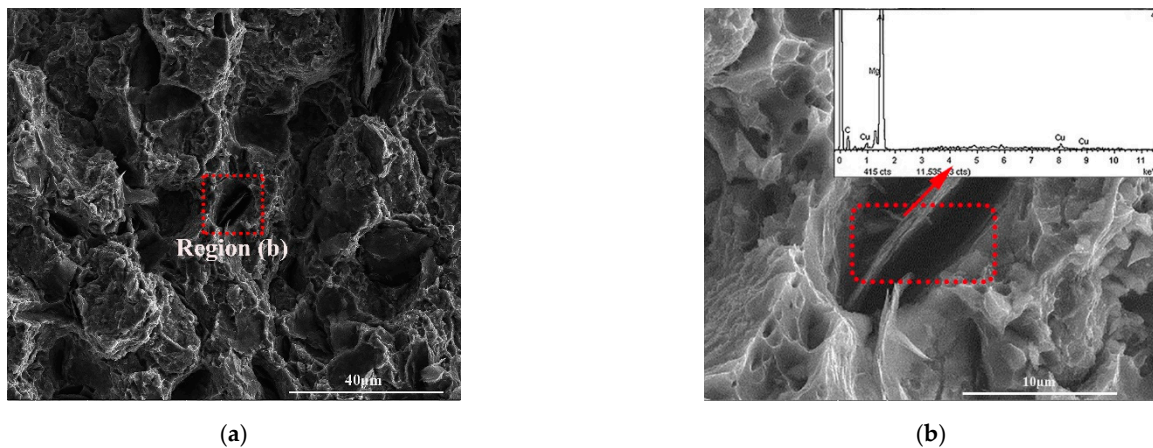


Figure 9. Cont.

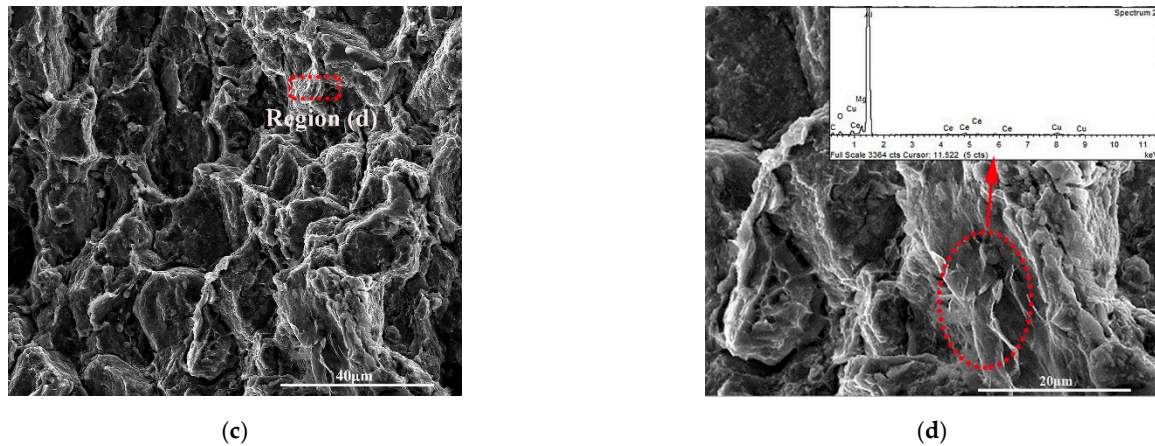


Figure 9. SEM images showing the fracture surfaces of the as-drawn (a,b) 0.5 wt.% GNPs/2024Al composites and (c,d) 0.5 wt.% CeO₂-GNPs/2024Al composites.

Coefficient of thermal expansion (CTE) mismatch strengthening, load transfer, and grain refinement mechanisms are considered to be the three main strengthening mechanisms for graphene-reinforced metal matrix composites. Coefficient of thermal expansion (CTE) mismatch strengthening refers to the enhancement of the mechanical properties due to the huge difference in the coefficient of thermal expansion (CTE) between GNPs and Al alloys promoting the generation of dislocations at the interfaces. The TEM image of dislocations is formed in the CeO₂-GNPs/2024Al composite, as shown in Figure 10.

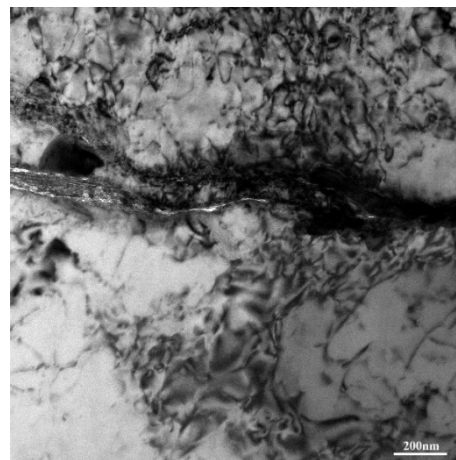


Figure 10. TEM image of dislocation in the composite fabricated.

Load transfer mechanism, in addition, is considered to be the critical mechanism with the greatest contribution to matrix strengthening among them. It mainly refers to the load transfer from the matrix to GNPs during the deformation of the composites. Furthermore, it can also be seen from Figure 6 that the addition of GNPs promoted grain refinement, which is beneficial to the improvement of the mechanical properties of the composites. Correspondingly, all three of them can be used to calculate the yield strength increase numerically through their calculation models. The contribution of these three mechanisms to the YS value improvement of composites are used to be numerically calculated through their corresponding calculation models frequently [26–28]:

$$\sigma_{CET} = 1.25Gb \sqrt{\frac{12\Delta T \Delta C f_v}{bd_p}}, \quad (1)$$

$$\Delta\sigma_{hall-patch} = K(d_{com}^{-1/2} - d_{matrix}^{-1/2}), \quad (2)$$

$$\Delta\sigma_{LT} = \frac{f_v}{2} \sigma_m, \quad (3)$$

where G is the shear modulus of Al (0.26×10^5 MPa), b is the burger vector of the matrix (0.286 nm), ΔT is the change value of temperature, ΔC is the CET difference value between Al matrix and GNPs, d_p represents the average diameter of GNPs, f_v is the volume fraction and average diameter of GNPs. In addition, d_{matrix} and d_{com} are the average grain sizes of the matrix and the composite fabricated, and K is the Hall–Petch coefficient of Al alloy. σ_m is denoted the YS of the matrix.

The theoretical YS contribution value calculated according to Equations (1)–(3) are shown in Figure 11. The comparison of Figure 11 exhibits that the theoretical YS value is much higher than the current experimental yield strength value. Moreover, the fine-grain strengthening mechanism contributes the lowest yield strength among the three strengthening mechanisms. The load transfer strengthening mechanism provides the main contribution. It confirms that the load transfer strengthening mechanism plays a major role in the performance improvement of the composites prepared, as mentioned above.

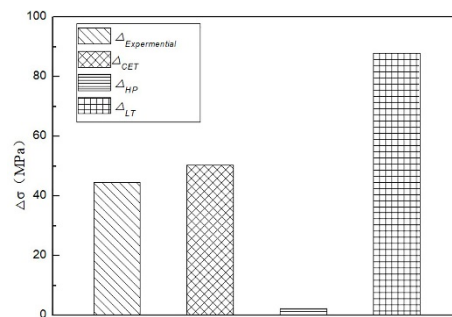


Figure 11. Comparison of the theoretical contribution for yield strength of composite with different strengthening mechanisms.

In fact, the results obtained through theoretical calculations mentioned above could only represent the maximum optimal value of YS. The discrepancy of the calculated and the actual values is mainly caused by two reasons: the uniform dispersion of GNPs in the matrix and strong interface bonding are the prerequisites for the effective role of strengthening mechanisms in composites. However, the existence of GNPs clusters causes that only part of the GNPs added to be stressed when the composites fabricated are subjected to tensile stress [29–31]. Moreover, the poor bonding force between the C-C layers or GNPs-matrix reduces the potential of GNPs to improve the strengthening of the matrix. In other words, the dispersion and wetting optimization of GNPs in the matrix is beneficial to the enhancement effect of GNPs on the mechanical properties of the composites. According to Figure 5, the composite reinforced with undecorated GNPs showed a more obvious tendency of GNPs agglomeration at the grain boundary as compared to the composites prepared by adding decorated GNPs. It is concluded that the decorating process is beneficial to disperse GNPs uniformly in the matrix alloy and improves its bonding and wettability with the matrix. As a result, the mechanical properties of composites fabricated have been further improved.

4. Conclusions

In order to explore the influence of the decorative effect of GNPs on the strengthening efficiency of GNPs/Al composites, GNPs were decorated with rare earth oxide CeO₂ and 0.5 wt.% CeO₂-GNPs/2024Al composites were successfully prepared. According to the results of microstructure observation and mechanical properties, the following conclusions can be drawn:

(1) Reinforcement GNPs decorated by CeO₂ particles were successfully prepared by the alcohol heating method. The rare earth oxides CeO₂ and GNPs were tightly bonded, and this combination was maintained after the composites were prepared by the pressure sintering process.

(2) The addition of CeO₂-GNPs showed a better grain refinement effect than the original GNPs for the composites fabricated with the same preparation conditions. Moreover, the load transfer mechanism is considered to be the critical mechanism to matrix strengthening.

(3) The effects of raw GNPs and CeO₂-GNPs on the mechanical properties of composites were investigated. Results exhibited that the performances of composite reinforced by CeO₂-GNPs are better than those values of the composite enforced with the raw GNPs of the same quality. The YS, UTS, and hardness of the composites were prepared by adding 0.5 wt.% CeO₂-GNPs are 184.1 MPa, 271.8 MPa, and 128 Hv, which are increased by 21.1%, 24.7%, and 26.7% compared to these of the matrix, respectively.

(4) The fracture interface showed the change from GNPs debonding to the tight bonding of GNPs to the matrix, indicating that the combination of the matrix and GNPs has been optimized due to the decorative effect of rare earth CeO₂. The optimization of interface bonding and distribution promotes GNPs to play a more effective role in a variety of strengthening effects, thereby significantly improving the mechanical properties of composites.

Author Contributions: Conceptualization, Z.G.; writing, Q.W.; formal analysis and data curation, S.L. and N.L.; Funding acquisition, Z.G. All authors have read and agreed to the published version of the manuscript.

Funding: This research was funded by Jiangxi Provincial key laboratory open fund project, grant number “EJ202003431” and Major Scientific and Technological Research and Development Projects in Jiangxi Province, grant number “20194ABC28001”.

Institutional Review Board Statement: Not applicable.

Informed Consent Statement: Not applicable.

Conflicts of Interest: The authors declare no conflict of interest.

References and Note

1. Wei, G.A.; Hz, A.; Wy, A.; Yin, Z.A.; Hua, Z.B.; Peng, P.A.; Fei, L.A.C. The microstructure and mechanical properties of C/C composite/Ti3Al alloy brazed joint with graphene nanoplatelet strengthened Ag-Cu-Ti filler. *Ceram. Int.* **2019**, *45*, 8783–8789.
2. Ramezanzade, S.; Ebrahimi, G.R.; Torabi-Parizi, M.; Ezatpour, H.R. Synergetic effect of GNPs and MgOs on the mechanical properties of Mg–Sr–Ca alloy. *Mater. Sci. Eng. A* **2019**, *761*, 138025. [[CrossRef](#)]
3. Medellín-Banda, D.L.; Navarro-Rodríguez, D.; Fernández-Tavizón, S.; Vila-Orta, C.A.; Comparán-Padilla, V.E. Enhancement of the thermal conductivity of polypropylene with low loadings of Cu-Ag alloy nanoparticles and graphene nanoplatelets. *Mater. Today Commun.* **2019**, *21*, 100695. [[CrossRef](#)]
4. Rashad, M.; Pan, F.; Liu, Y.; Chen, X.; Lin, H.; Pan, R. High temperature formability of graphene nanoplatelets-AZ31 composites fabricated by stir-casting method. *J. Magnes. Alloy.* **2016**, *4*, 270–277. [[CrossRef](#)]
5. Xu, R.; Zheng, X.; Chen, M.; Sun, L.; Ma, Y. Enhancing the linearity and stability of a fabric-based strain sensor with microfolded graphene structures. *Appl. Sci.* **2020**, *10*, 6230. [[CrossRef](#)]
6. Srivvyas, P.D.; Charoo, M.S. Tribological behavior of aluminum silicon eutectic alloy based composites under dry and wet sliding for variable load and sliding distance. *Appl. Sci.* **2020**, *2*, 1654.1–1654.21. [[CrossRef](#)]
7. Tao, J.; Wang, J.; Zeng, Q. A comparative study on the influences of CNT and GNP on the piezoresistivity of cement composites. *Mater. Lett.* **2020**, *259*, 126858.1–126858.4. [[CrossRef](#)]
8. Singh, S.; Sharma, S.; Keshri, A.K. Tribological Behaviour of Plasma-Sprayed Graphene Nanoplatelets Reinforced Hydroxyapatite Nanocomposite Coating. *Trans. Indian Inst. Met.* **2021**, *74*, 2901–2907. [[CrossRef](#)]
9. Kumar, A.P.; Madhu, H.C.; Pariyar, A.; Perugu, C.S.; Kailas, S.V.; Uma, G.; Pradeep, R. Friction stir processing of squeeze cast A356 with surface compacted graphene nanoplatelets (GNPs) for the synthesis of metal matrix composites. *Mater. Sci. Eng.* **2020**, *769*, 138517.1–138517.10.
10. Cai, Z.; Zhang, F.; Yang, C.; Wang, X.X.; Long, Y.Z. Graphene quantum dots doped pvdf(tbt)/pvp(tbt) fiber film with enhanced photocatalytic performance. *Appl. Sci.* **2020**, *10*, 596.
11. Srivvyas, P.D.; Charoo, M.S. Tribological behaviour of nano additive based PAO lubricant for eutectic Al-Si alloy-chromium plated chrome steel tribopair. *Mater. Today Proc.* **2020**, *44*, 1–6. [[CrossRef](#)]
12. Li, J.; Zhang, X.; Geng, L. Improving graphene distribution and mechanical properties of GNP/Al composites by cold drawing. *Mater. Des.* **2018**, *144*, 159–168. [[CrossRef](#)]
13. Sharma, A.; Sharma, V.M.; Sahoo, B.; Surjya, K.P.; Jinu, P. Effect of multiple micro channel reinforcement filling strategy on A16061-graphene nanocomposite fabricated through friction stir processing. *J. Manuf. Process.* **2019**, *37*, 53–70. [[CrossRef](#)]

14. Li, J.; Zhang, X.; Geng, L. Effect of heat treatment on interfacial bonding and strengthening efficiency of graphene in GNP/Al composites. *Compos. Part A Appl. Sci. Manuf.* **2019**, *121*, 487–498. [[CrossRef](#)]
15. Sharma, A.; Sharma, V.M.; Paul, J. A comparative study on microstructural evolution and surface properties of graphene/CNT reinforced Al6061SiC hybrid surface composite fabricated via friction stir processing. *Trans. Nonferrous Met. Soc. China* **2019**, *29*, 2005–2026. [[CrossRef](#)]
16. Jjxa, B.; Hong, Y. Microstructure and mechanical properties of ADC12 composites reinforced with graphene nanoplates prepared by ultrasonic assisted casting. *Trans. Nonferrous Met. Soc. China* **2020**, *30*, 3210–3225.
17. Yuan, Q.H.; Zhou, G.H.; Liao, L.; Liu, Y.; Luo, L. Interfacial structure in AZ91 alloy composites reinforced by graphene nanosheets. *Carbon Int. J. Spons. Am. Carbon Soc.* **2018**, *127*, 177–186. [[CrossRef](#)]
18. Park, Y.; Cho, K.; Park, I.; Park, Y. Fabrication and mechanical properties of magnesium matrix composite reinforced with si coated carbon nanotubes. *Procedia Eng.* **2011**, *10*, 1446–1450. [[CrossRef](#)]
19. Yuan, Q.; Zeng, X.; Wang, Y.; Luo, L.; Ding, Y.; Li, D.; Liu, Y. Microstructure and mechanical properties of Mg-4.0Zn alloy reinforced by NiO-coated CNTs. *J. Mater. Sci. Technol.* **2017**, *33*, 452–460. [[CrossRef](#)]
20. Yuan, Q.H.; Qiu, Z.Q.; Zhou, G.H.; Zeng, X.S.; Luo, L.; Rao, X.X. Interfacial design and strengthening mechanisms of az91 alloy reinforced with in-situ reduced graphene oxide. *Mater. Charact.* **2018**, *138*, 215–228. [[CrossRef](#)]
21. Joint Committee on Powder Diffraction Standards (JCPDS). International Centre for Diffraction Data. PCPDFWIN. 2002.
22. Kumar, H.G.P.; Prabhakaran, S.; Xavior, M.A.; Kalainathan, S.; Lin, D.; Shukla, P.; Vasudevan, V.K. Enhanced surface and mechanical properties of bioinspired nanolaminate graphene-aluminum alloy nanocomposites through laser shock processing for engineering applications. *Mater. Today Commun.* **2018**, *16*, 81–89.
23. Hccab, C.; Yllab, C. The microstructures and mechanical properties of graphene-reinforced titanium matrix composites. *J. Alloy. Compd.* **2021**, *812*, 152057.
24. Wu, L.; Wu, R.; Hou, L.; Zhang, J.; Zhang, M. Microstructure, mechanical properties and wear performance of AZ31 matrix composites reinforced by graphene nanoplatelets(gnps). *J. Alloy. Compd.* **2018**, *750*, 530–536. [[CrossRef](#)]
25. Li, N.; Yan, H.; Wu, Q. Fabrication of Carbon Nanotubes and Rare Earth Pr Reinforced AZ91 Composites by Powder Metallurgy. *Chin. J. Mech. Eng.* **2021**, *2*, 213–222. [[CrossRef](#)]
26. Rashad, M.; Pan, F.; Tang, A.; Asif, M.; Hussain, S.; Gou, J.; Mao, J.J. Improved strength and ductility of magnesium with addition of aluminum and graphene nanoplatelets (Al+GNPs) using semi powder metallurgy method. *J. Ind. Eng. Chem.* **2015**, *23*, 243–250. [[CrossRef](#)]
27. Rashad, M.; Pan, F.; Asif, M.; Tang, A. Powder metallurgy of Mg–1%Al–1%Sn alloy reinforced with low content of graphene nanoplatelets (GNPs). *J. Ind. Eng. Chem.* **2014**, *20*, 4250–4255. [[CrossRef](#)]
28. Miller, W.; Humphreys, F. Strengthening mechanisms in particulate metalmatrix composites: Reply to comments by Arsenault. *Scr. Metal. Mater.* **1991**, *25*, 2623–2626. [[CrossRef](#)]
29. Bisht, A.; Srivastava, M.; Kumar, R.M.; Lahiri, I.; Lahiri, D. Strengthening mechanism in graphene nanoplatelets reinforced aluminum composite fabricated through spark plasma sintering. *Mater. Sci. Eng. A* **2017**, *695*, 20–28. [[CrossRef](#)]
30. Xiong, B.; Gang, L. Effects of graphene content on microstructures and tensile property of graphene-nanosheets/aluminum composites. *J. Mater. Sci. Solid State Chem. Phys.* **2017**, *697*, 31–36.
31. Enel, M.C.; Gurbuz, M.; Ko, E. Effect of graphene content on tensile strength and microstructure of aluminum matrix composites. *Univers. J. Mater. Sci.* **2018**, *6*, 79–84.